Timing evidence in determining the accretion state of the Seyfert galaxy NGC 3783

D. P. Summons[1,3]⋆, P. Arévalo[1] , I. M. McHardy[1], P. Uttley[2] and A. Bhaskar[3]

[1]*School of Physics and Astronomy, University of Southampton, Southampton SO17 1BJ, UK*
[2]*Astronomical Institute 'Anton Pannekoek', University of Amsterdam, Kruislaan 403, 1098 SJ, Amsterdam, the Netherlands*
[3]*School of Engineering Science, University of Southampton, Southampton SO17 1BJ, UK*

ABSTRACT
Previous observations with the *Rossi X-ray Timing Explorer* (*RXTE*) have suggested that the power spectral density (PSD) of NGC 3783 flattens to a slope near zero at low frequencies, in a similar manner to that of Galactic black hole X-ray binary systems (GBHs) in the 'hard' state. The low radio flux emitted by this object, however, is inconsistent with a hard state interpretation. The accretion rate of NGC 3783 ($\sim 7\%$ of the Eddington rate) is similar to that of other AGN with 'soft' state PSDs and higher than that at which the GBH Cyg X-1, with which AGN are often compared, changes between 'hard' and 'soft' states ($\sim 2\%$ of the Eddington rate). If NGC 3783 really does have a 'hard' state PSD, it would be quite unusual and would indicate that AGN and GBHs are not quite as similar as we currently believe. Here we present an improved X-ray PSD of NGC 3783, spanning from $\sim 10^{-8}$ to $\sim 10^{-3}$ Hz, based on considerably extended (5.5 years) *RXTE* observations combined with two orbits of continuous observation by *XMM-Newton*. We show that this PSD is, in fact, well fitted by a 'soft' state model which has only one break, at high frequencies. Although a 'hard' state model can also fit the data, the improvement in fit by adding a second break at low frequency is not significant. Thus NGC 3783 is not unusual. These results leave Arakelian 564 as the only AGN which shows a second break at low frequencies, although in that case the very high accretion rate implies a 'very high', rather than 'hard' state PSD. The break frequency found in NGC 3783 is consistent with the expectation based on comparisons with other AGN and GBHs, given its black hole mass and accretion rate.

Key words: galaxies: active – galaxies: Seyfert – galaxies: NGC 3783 – X rays: galaxies

1 INTRODUCTION

Super-massive black holes in active galactic nuclei (AGN) and Galactic stellar-mass black hole X-ray binary systems (GBHs) both display aperiodic X-ray variability which may be quantified by calculating the power spectral densities (PSDs) of the X-ray light curves. The PSDs can typically be represented by red-noise type power laws (i.e. $P(\nu)$, the power at frequency ν, $\propto \nu^{\alpha}$ where $\alpha \sim$ -1) with a bend or break (to $\alpha \leqslant$ -2) at a characteristic PSD frequency. The time-scale, corresponding to the bend-frequency, scales approximately linearly with black hole mass from AGN to GBHs (McHardy 1988; Edelson & Nandra 1999; Uttley et al. 2002, 2005; Markowitz et al. 2003; McHardy et al. 2004, 2005), albeit

with some scatter. However, the scatter is entirely accounted for by variations in accretion rate, allowing scaling between AGN and GBHs on time-scales from $\sim$ years to $\sim$ ms (McHardy et al. 2006).

GBHs are observed in a number of distinct X-ray spectral states which also have distinct X-ray timing properties. Two common states are the low/hard (hereafter 'hard') and high/soft (hearafter 'soft') states. In the hard state, the energy-spectrum is dominated by a highly variable power law component and the PSDs are well fitted by multiple broad Lorentzians. For use in AGN, where signal/noise is lower than in GBHs, this PSD shape can be approximated by a double-bend power law with slopes $\alpha = 0$, -1 and -2, from low to high frequency, where the high- and low-frequency bends correspond to the strongest peaks in the Lorentzian parameterisation. The breaks are typically separated by only one to two decades in frequency. In the soft state, the en-

ergy spectrum is dominated by an approximately constant thermal disc component which extends into the X-ray band in GBHs but which in AGN is shifted down to the optical/UV band. Therefore, a meaningful comparison between the PSDs of soft state GBH and AGN can only be made in cases where the GBH power-law emission is strong enough to show significant variability. Such GBHs are rare and the best example is Cyg X-1 which shows a '1/f' PSD over many decades of frequencies (Reig et al. 2002). The soft state is distinguished from the hard state by having only one, high frequency, break in this power law, from slope -1 to -2.

It has been suggested that this pure simple broken or cut-off power-law PSD shape is unique to the soft state of Cyg X-1, which is a persistent source. However in transient GBHs with similar X-ray spectra, the power law PSD component may be seen in combination with broad Lorentzian features (Done & Gierliński 2005). Axelsson et al. (2006) also note that a mixed power law plus Lorentzian PSD is also present in Cyg X-1 in lower luminosity, harder spectral states, but as the luminosity rises the Lorentzian features weaken and the power law PSD component strengthens until, in the softest state, it completely dominates. Since the softest spectral states of transient GBHs are dominated by constant disc emission we cannot determine whether they show a similar PSD shape to Cyg X-1.

However, a direct comparison of transient GBHs and Cyg X-1 is complex, since the transients show much larger luminosity changes, and complex hysteresis effects in spectral hardness versus luminosity (e.g. Homan et al. 2001, Belloni et al. 2005) which are not seen in Cyg X-1. Therefore it is not clear that one can compare timing properties between Cyg X-1 and transient GBHs simply as a function of observed X-ray spectrum.

None the less, it is still interesting that the X-ray spectrum of Cyg X-1 never becomes totally disc-dominated, and always contains a relatively strong variable component whose PSD resembles that of X-ray bright AGN. If variability originates, at least partly, in the disc, so power spectral shape is related to the disc structure, that structure might be severely disrupted during outbursts, thereby suggesting a possible difference between the persistent Cyg X-1 and the transient GBH sources. The similarities between the PSDs of Cyg X-1 and AGN may also be related to the possible similarities in accretion flows between AGN and Cyg X-1 noted by Done & Gierliński (2005).

To date, NGC 3783 and the Narrow Line Seyfert 1 Galaxy (NLS1) Ark 564 are the only AGN with suggested second, low-frequency breaks in their PSDs (i.e. similar to low/hard GBHs) and are both commonly referred to as being unusual (e.g. Done & Gierliński 2005). The power spectral evidence for a second break in the case of Ark 564 is very strong (Pounds et al. 2001; Papadakis et al. 2002; Markowitz et al. 2003, McHardy et al. in prep.). Of all the AGN with good timing data, Ark 564 shows the highest accretion-rate (possibly super-Eddington) so it would not be surprising if it were in an unusual state, e.g. the 'very high' state where the PSD, in GBHs, also displays two distinct breaks. The properties of NGC 3783, on the other hand, are similar to those of AGN with proven soft-state PSDs (e.g. NGC 3227, NGC 4051 McHardy et al. 2004, MCG-6-30-15 McHardy et al. 2005), and in particular it is radio quiet (e.g. Reynolds 1997). In the hard state, GBHs are strong

radio sources whereas in the soft state the radio emission is quenched (Corbel et al. 2000; Fender 2001; Körding et al. 2006). We also note that NGC 3783 has a more moderate accretion rate than Ark 564 ($\sim 7\%$), and more similar to the other AGN mentioned above, and Cyg X-1 changes from the hard to the soft state at around 2% of the Eddington accretion rate (i.e. $\dot{m}_E =0.02$) (Pottschmidt et al. 2003; Wilms et al. 2006; Axelsson et al. 2006). These two facts do not lie easily with a hard state identification of NGC 3783. Thus it would be surprising, and might indicate that our current ideas regarding the scaling between AGN and GBHs are not entirely correct, if NGC 3783 were proven to have a hard state PSD. It is therefore important to determine whether NGC 3783 does have a second, low frequency, break in its PSD or not.

Markowitz et al. (2003) recognised the presence of a break in the $2 - 10$ keV PSD of NGC 3783 at 4×10^{-6} Hz and found provisional evidence for a second lower-frequency break at $\sim 2\times10^{-7}$ Hz. Specifically, Markowitz et al. (2003) rejected the possibility that the PSD is described by a single-break power law with low-frequency slope -1, similar to other AGN, at the 98% confidence level. In this paper we re-investigate the evidence for the second break in the PSD of NGC 3783, using new long-term monitoring data that covers the frequency range where the break appears to be. By including additional *RXTE* archival data spanning several years, along with short time-scale observations by *XMM-Newton*, we will demonstrate that the improved PSD is perfectly compatible with a single-bend power law, consistent with the behaviour of the other moderately-accreting Seyferts. In Section 2 we describe the observations and the methods by which we extract the *RXTE* and *XMM-Newton* light curves. In Sections 3 we discuss the PSD of NGC 3783 as produced from the *RXTE* and *XMM-Newton* observations, and compare it with various PSD models. In Section 4 we briefly review the implications of our observations.

2   OBSERVATIONS AND DATA REDUCTION

2.1   *RXTE* Data Reduction

From 1999 to 2006, NGC 3783 has been the target of various monitoring campaigns with *RXTE*. These campaigns have consisted of short, $\sim$1 ks duration, observations with the proportional counter array (PCA, Zhang et al. 1993). We have analysed the archival PCA STANDARD-2 data and our own proprietary data with FTOOLS v6.0.2 using standard extraction methods. We use data from the top layers of PCUs 0 and 2 up to 2000 May 12 and only top layer PCU 2 data from observations after this date. The remaining PCUs were not used due to repeated breakdowns.

Data were selected according to the standard 'good-time' criteria, i.e. target elevation $< 10°$, offset pointing $< 0.02°$, and electron contamination < 0.1. The background was simulated with the L7 model for faint sources using PCABACKEST v3.0. The response matrices for each PCA observation were calculated using PCARSP v10.1. The final $2 - 10$ keV fluxes were calculated using XPSEC v12.2.1 by fitting a power law with galactic absorption to the PHA data.

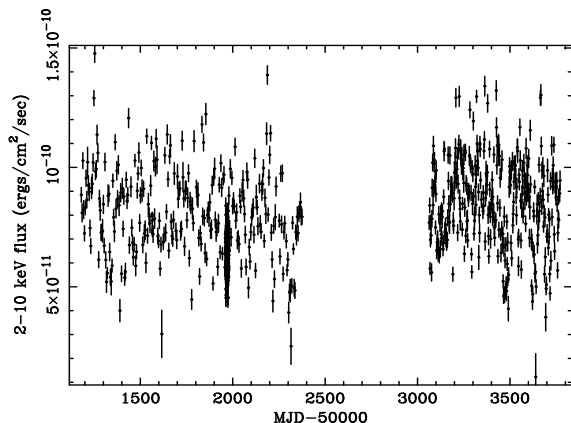The *RXTE* data used in our analysis, together with the

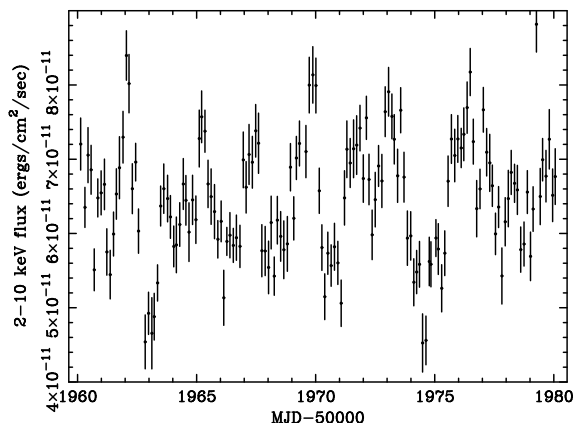**Figure 1.** *RXTE* long-term light curve of NGC 3783 in the 2-10keV band.

Figure 2. *RXTE* intense sampling light curve in the 2-10 keV band of NGC 3783.

sampling patterns, are listed in Table 1 and displayed in Fig. 1. The early data (to MJD 52375) with 4 d sampling, together with the 20 d period of 3 h sampling already presented by Markowitz et al. (2003) are followed, after a 2 year gap, by our new long-term monitoring, with 2 d sampling. As the gap is large compared to the duration of each monitoring campaign we will include data from each monitoring campaign as separate lightcurves in our fits.

2.2   *XMM-Newton* **Data Reduction**

NGC 3783 was observed by *XMM-Newton* during revolutions 371 and 372, between 2001 December 17 and 2001 December 21. Temporal analysis of these data were first presented by Markowitz (2005) who discusses the coherence, frequency-dependent phase lags, and variation of high frequency PSD slope with energy. Here we use these data to constrain the high frequency part of the overall long and short timescale PSD. We used data from the European Photon Imaging Cameras (EPIC) PN and MOS2 instruments, which were operated in imaging mode. MOS1 was operated in Fast Uncompressed Mode and we do not use those data here. The PN camera was operated in Small Window mode, using the medium filter. Source photons were extracted from a circular region of $40''$ radius and the background was se-
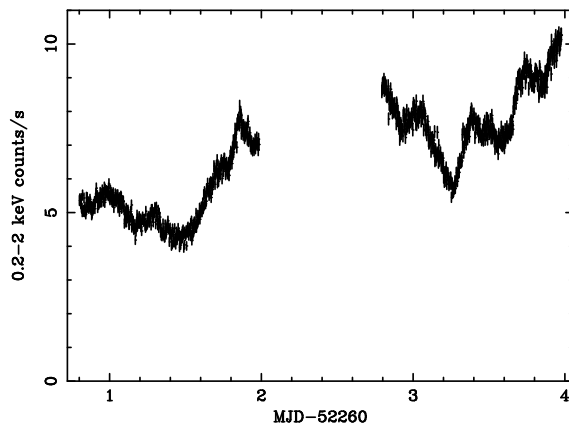

Figure 3. *XMM-Newton* light curve in the 0.2–2 keV band of NGC 3783.

lected from a source-free region of equal area on the same chip. We selected single and double events, with quality flag=0. The MOS2 camera was operated in the Full Window mode, using the medium filter. We extracted source and background photons using the same procedure as for the PN data and selected single, double, triple and quadruple events. These data showed no serious pile-up when tested with the *XMM-SAS* task *epatplot*.

We constructed light curves, for each detector and orbit, in the 0.2–2, 2–10 and 4–10 keV energy bands. We filled in the ~ 5 ks gap in the middle of orbit 371 light curves, and some other much smaller gaps, by interpolation and added Poisson noise. The resulting PN and MOS2 continuous light curves were then combined to produce the final light curves for each orbit. The combined, background subtracted, average count rates in the 0.2–10 keV band were 11.8 c/s for orbit 371 and 15.8 c/s for orbit 372, and the 0.2-2 keV combined light curve is shown in Fig. 3. Poisson noise dominates the PSD on timescales shorter than 1000s, so the light curves were binned into 200s bins.

3   POWER SPECTRAL MODELLING

3.1   **Combining** *RXTE* **and** *XMM-Newton* **data**

To determine the PSD over the largest possible frequency range we combine the *RXTE* and *XMM-Newton* data. In GBHs the break-frequency and slope of the PSD below the break appear to be independent of the chosen energy band (Cui et al. 1997; Churazov et al. 2001; Nowak et al. 1999; Revnivtsev et al. 2000; McHardy et al. 2004). On the other hand, the PSD normalisation and the slope above the break are often energy-dependent (Markowitz 2005). Therefore, when combining data from different instruments, it is preferable to use similar energy ranges. The *RXTE* data are in the 2–10 keV band and, for NGC 3783, that band has a median photon energy of 5.7 keV. The *XMM-Newton* band with the same median photon energy is 4.1–10 keV. However the count rate in that *XMM-Newton* band is low (2 c/s) so we only detect significant source power above the Poisson noise level at frequencies below 10^{-4}Hz. To probe higher frequencies we can use the 0.2–2 keV *XMM-Newton* data (8.8 c/s) but we must re-scale its PSD normalisation to

Light curve	Sampling interval	Observation length	Date Range [MJD]
RXTE Long-term 1	∼4.36 days	1194.6 days	51180.5–52375.1
RXTE Long-term 2	∼2.1 days	928.3 days	53063.4–53991.6
RXTE Intense monitoring	∼3.2 hours	19.9 days	51960.1–51980.1
XMM-Newton observations (2 orbits)	200-s	3.2 days	52260.8–52264.0

Table 1. Summary of the *RXTE* and *XMM-Newton* light curves used in the analysis of NGC 3783, including their sampling frequency and date range.

that of the 4–10 keV PSD. We determined the scaling correction by producing PSDs in both energy bands and fitting the same bending power law model to the noise-subtracted data. On the assumption that the PSD shape below the high frequency break is energy-independent, the combined *RXTE* 2–10 keV and *XMM-Newton* 0.2–2 keV PSD will then have the shape of the 0.2–2 keV PSD.

3.2 Monte Carlo simulations

We use the Monte Carlo technique of Uttley et al. (2002) (PSRESP), to estimate the underlying PSD parameters in the presence of sampling biases. In this method we first calculate the observed (or 'dirty') PSD, in parts, from the observed lightcurves, using the Discrete Fourier Transform. Here the PSD estimates are binned in bins of width 1.3ν, where ν is the starting frequency by taking the average of the log of power (Papadakis & Lawrence 1993). We require a minimum of 4 PSD estimates per bin. We then compare simultaneously the dirty PSDs from each lightcurve with various model PSDs derived from lightcurves simulated with the same sampling pattern as the real observations. We alter the model parameters to obtain the best fit for any given model. We refer the reader to Uttley et al. (2002) for a full discussion of the method.

For each set of chosen underlying-PSD model parameters, we simulate red-noise light curves, as described by Timmer & Koenig (1995). The *RXTE* light curves are simulated with time resolutions of 10.5 h, 5.0 h and 18 m for the first and second long time-scale and the medium time-scale light curves respectively. The simulated resolution, which is 10 times shorter than the typical sampling intervals of the real observations, given in column 2 of Table 1, is to take into account the effect of aliasing. These simulated light curves were resampled and binned to match the real NGC 3783 observations. *XMM-Newton* light curves were simulated with 200-s resolution, as at shorter time-scales the underlying varability power is negligible compared to the Poisson noise, so aliasing does not play a role. The Poisson noise level was not subtracted from the observed PSD but was added to the simulated PSDs. To reproduce the effect of red-noise leak, each light curve was simulated to be ∼300 times longer than the real observation, and was then split into sections, constituting 300 simulated light curves for each observed lightcurve. The simulated model average PSD is evaluated from this ensemble of PSD realisations, and the errors are assigned from the rms spread of the realisations within a frequency bin.

We present the results of several PSD model fits in an attempt to quantify the underlying model shape that best describes the PSD of NGC 3783, and associate an accep-
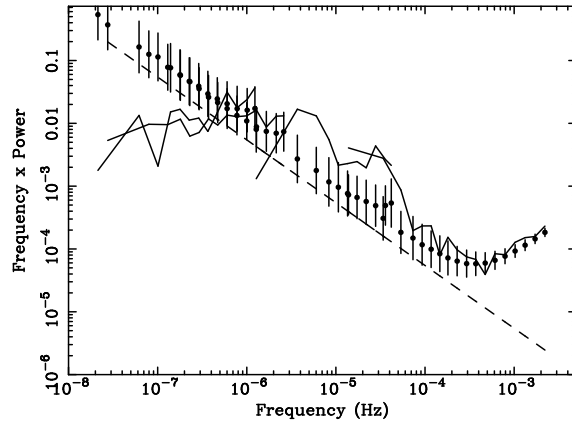

Figure 4. The best fit unbroken power law PSD of the combined *RXTE* and *XMM-Newton* data. The solid lines represent the observed data and the points with error bars exhibit the biased model and the spread in individual realisations of the model. The dashed line is the underlying model used to generate the simulated PSD. The three lowest frequency data sets are from *RXTE* observations and the high frequency data set ($\sim 10^{-5}$ Hz) is from the *XMM-Newton* observations. Note that the rise in power at the highest frequencies is due to the photon Poisson noise.

tance probability with each model. We initially test a simple unbroken power law model. We next fit a power law with a single-bend in the PSD, and then a model incorporating a double-bend. We also fit a single-bend power law with a Lorentzian component.

3.3 Unbroken power law model

To begin, we fitted a simple power law model to the data of the form:

$$P(\nu) = A \left(\frac{\nu}{\nu_0} \right)^{\alpha}$$

where A is the normalisation at a frequency ν_0, and α is the power law slope. We made 900 simulations and in Fig. 4 we show the best fit plotted in $\nu \times P_\nu$, which has a PSD slope of -2.1. However, the fit is poor and this model can be rejected with a probability > 99 %, or $\gtrsim 3\,\sigma$.

3.4 Single-bend power law model

Here we fit a single-bend power law to the data. This model best describes the PSD of Cyg X-1 in the high/soft state, and provides a good fit to the PSDs of the AGN NGC 4051 and MCG–6-30-15 (McHardy et al. 2004, 2005).
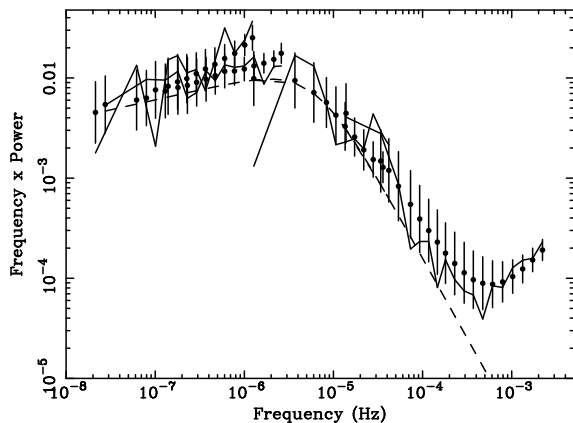
Figure 5. The best fit single-bend power law PSD of the combined *RXTE* and *XMM-Newton* data. The various lines represent the same data as seen in Fig. 4.
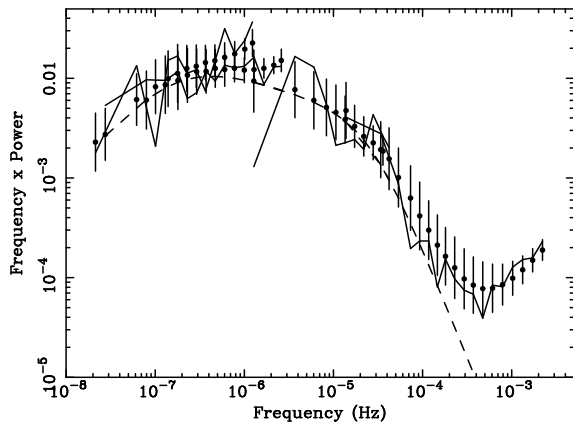

Figure 6. The best fit double-bend power law PSD of the combined *RXTE* and *XMM-Newton* data. The various lines represent the same data as seen in Fig. 4.

$$P(\nu) = \frac{A\,\nu^{\alpha_L}}{1 + \left(\frac{\nu}{\nu_B}\right)^{\alpha_L - \alpha_H}}$$

Fig. 5 presents the observed PSD fitted with a single-bend power law model, for which a good likelihood of acceptance is obtained (P = 44 %). The best fit bend-frequency is $\nu_B = 6.2^{+40.6}_{-5.6} \times 10^{-6}$ Hz, the high-frequency slope is $\alpha_H = -2.6^{+0.6}_{-*}$, and the low-frequency slope is $\alpha_L = -0.8^{+*}_{-0.5}$. The errors are 90% confidence limits, an asterisk indicates that the limit is unconstrained. For α_H the best fit value is well within the searched parameter space but the degeneracy produced by red-noise leak in the probability at high values of α_H, means that the upper limit is not constrained at the 90% confidence level. The confidence contours for the main interesting parameters are plotted in Figs. 7 and 8. Table 2 shows the single-bend power law best fit parameters to the data. The best fit single-bend frequency obtained here is consistent with the value found by Markowitz et al. (2003)

3.5 Double-bend power law model

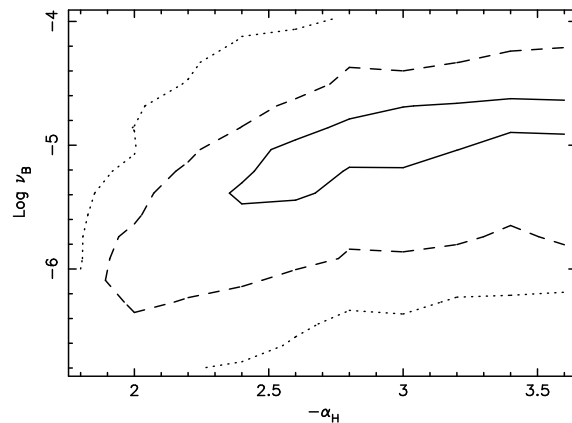Markowitz et al. (2003) provide tentative evidence that

Figure 7. Single-bend power law model: 68, 90, and 99% confidence contours for the bend frequency, ν_B, and the high frequency slope, $-\alpha_H$, for the single-bend power law fit to the combined *RXTE* and *XMM-Newton* PSD.
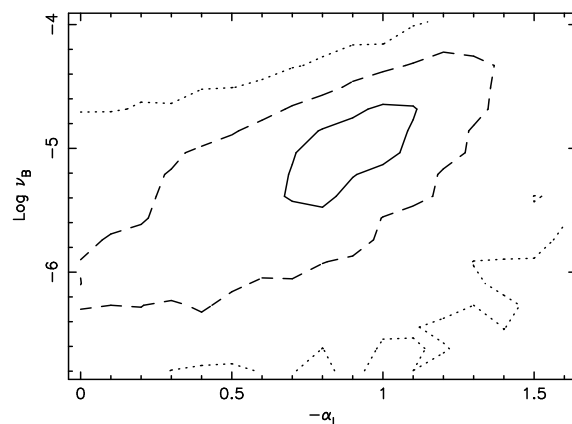

Figure 8. Single-bend power law model: 68, 90, and 99% confidence contours for the bend frequency, ν_B, and the low frequency slope, $-\alpha_L$, for the single-bending power law fit to the combined *RXTE* and *XMM-Newton* PSD.

a second, lower, frequency break exists in the PSD of NGC 3783. Thus, we also fitted a more complex double-bend power law model to see if the goodness-of-fit is improved significantly. The double-bend power law model is given by:

$$P(\nu) = \frac{A\,\nu^{\alpha_L}}{\left[1 + \left(\frac{\nu}{\nu_L}\right)^{\alpha_L - \alpha_I}\right]\left[1 + \left(\frac{\nu}{\nu_H}\right)^{\alpha_I - \alpha_H}\right]},$$

where α_I is the intermediate-frequency slope and ν_L and ν_H are the low and high bend-frequencies respectively. We fixed the low-frequency slope to zero, to avoid making the simulations computationally prohibitive, and because a low-frequency slope of zero would allow the best qualitative comparison to the low state of Cyg X-1 (Nowak et al. 1999).

Fig. 6 presents the same observed PSD as in Fig. 5, but fitted with the double-bend power law model. A good likelihood of acceptance is obtained (P=64 %). The best-fitting high bend-frequency is $\nu_H = 2.6^{+*}_{-*} \times 10^{-5}$ Hz, the high-frequency slope is $\alpha_H = -3.2^{+1.2}_{-*}$, the intermediate-frequency slope is $\alpha_I = -1.3^{+*}_{-*}$, the low-frequency bend is $\nu_L = 1.7^{+*}_{-*} \times 10^{-7}$ Hz. As before, we use 90% confidence lim-

Model	Normalisation (a)	α_H	α_I	α_L	ν_H (Hz)	ν_L (Hz)	Acceptance (%)
Single-bend	1.5×10^{-4}	$-2.6^{+0.6}_{-1.0}$	NA	$-0.8^{+0.8}_{-0.5}$	$6.2^{+40.6}_{-5.6} \times 10^{-6}$	NA	44.4
Double-bend	1.0×10^{2}	$-3.2^{+1.2}_{-*}$	-1.3^{+*}_{-*}	0.0	$2.6^{+*}_{-*} \times 10^{-5}$	$1.7^{+*}_{-*} \times 10^{-7}$	63.9

Table 2. Best fit model parameters for the examined models to the combined *RXTE* and *XMM-Newton* PSD of NGC 3783. The errors on the single- and double-bend fits are calculated from the 90% confidence intervals. The bend-frequency for the single-bend model, ν_B, is denoted here as ν_H. An asterisk indicates that the limit is unconstrained.

its. The added parameters allow extra freedom to find better fit probabilities for any given set of double-bend parameters. For this reason, the contour levels cover larger ranges in the parameter space and therefore, most of the 90% contours in our double-bend fit remain unbounded over the fitted parameter space. The high-frequency slope is subject to the same problems as in the single-bend model. Table 2 contains a summary of the best-fitting model parameters.

The best-fitting low-frequency bend is found close to the lowest frequencies probed by the data and, as seen in Fig. 9, it is essentially unbounded down to the lowest measurable frequency at the 68% confidence level. These facts suggest that the second, low-frequency, bend might not be required by the data and that the improvement in the fit might be only due to the increased complexity of the model fitted.

The likelihood of acceptance is better in the double-bend model than in the single-bend model, 64 versus 44 % respectively, but there are more free parameters. In order to determine the significance of this improvement, we performed the following test. Using the best-fitting single-bend PSD parameters, we generated 300 realisations of the sets of *RXTE* and *XMM-Newton* lightcurves. Each realisation was then fitted with the best-fitting double-bend parameters, exactly as was done with the real data, and the distribution of their fit probabilities was constructed. We found that 121 out of the 300 single-bend simulations have a higher fit probability than the real data, when fitted with the double-bend model. Therefore, we conclude that the improvement in fit probability is no more than may be expected from fitting a model which is more complicated than required by the data: the double-bend model does not represent a significant improvement.

3.6   Single-bend power law with a Lorentzian component

We finally consider whether the observed PSD might be best-described by adding a Lorentzian component, such as are commonly used to describe broad-band noise components in GBHs (e.g. Nowak 2000), to the single-bend power law. We are motivated to consider this possibility because the PSD of the intense-sampling *RXTE* light curve is not very well described by either the single- or double-bend power law model. Visual inspection of this light curve, shown in Fig. 2, suggests that the variability is strongly concentrated on time-scales of around a day, or equivalently, frequencies around 10^{-5} Hz, which is confirmed by the peak seen in the corresponding section of the PSD, and the drop in the same PSD at lower frequencies ($\sim 10^{-6}$ Hz). The long-term monitoring PSDs, however, do not show a dip at 10^{-6} Hz, creating a large discrepancy in the PSD mea-
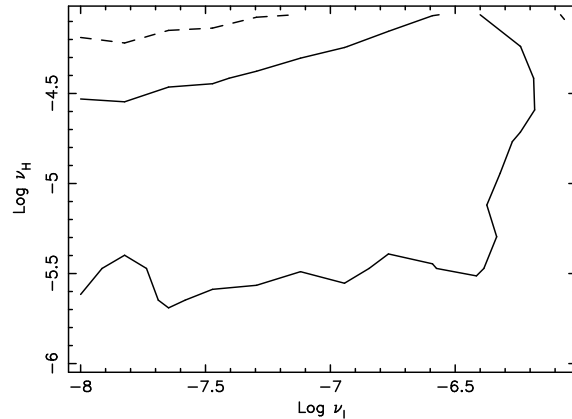

Figure 9. Double-bend power law model: 68, and 90% confidence contours for the high bend-frequency, ν_H, and the low bend-frequency, ν_L, for the double-bend power law fit to the combined *RXTE* and *XMM-Newton* PSD.

surements at this frequency. A strongly peaked component in the underlying PSD, at $\sim 10^{-5}$ Hz, could produce the observed features. Such a component would appear as a peak in a PSD that covered frequencies above and below its peak-frequency, but would be insufficiently sampled by the long-term monitoring campaigns; thus, its power would be aliased into the highest frequencies of the longer time-scale data, making them rise above the underlying model level and causing the apparent disparity.

The Lorentzian profile is described by:

$$P_{\mathrm{Lor}}(\nu) = \frac{AQ\nu_c}{\nu_c^2 + 4Q^2(\nu_c - \nu)^2},$$

where the centroid frequency ν_c is related to the peak-frequency ν_p by $\nu_p = \nu_c\sqrt{1 + 1/4Q^2}$ and the quality factor Q is equal to ν_c divided by the full width at half maximum of the Lorentzian. The variable A parameterizes the relative contribution of the power law and Lorentzian components to the total rms. Fitting a Lorentzian component in addition to a single-bend power law provides a good fit (P=52 %). The best-fitting Lorentzian contributes 20% of the variance in the frequency range probed and its best-fitting parameters are quoted in Table 3. Fig. 10 shows the observed PSD compared with the best-fitting single-bend power law model plus a Lorentzian component. The Lorentzian feature in the model can reproduce qualitatively the spurious power at the high frequency end of the long-term monitoring data and the turn down effect observed in the intensive-sampling data.

To determine the significance of the Lorentzian component fit we repeated the procedure used in determining the

ν_p (Hz)	ν_B (Hz)	Q	A	α_L	α_H	Acceptance (%)
$4.8^{+*}_{-0.8} \times 10^{-6}$	$1.1^{+0.6}_{-0.4} \times 10^{-5}$	$5.1^{+*}_{-3.6}$	$0.9^{+*}_{-0.7}$	-1.0^{+*}_{-*}	-2.6^{+*}_{-*}	52.3

Table 3. Best fit single-bend power law with Lorentzian component model parameters to the combined *RXTE* and *XMM-Newton* PSD of NGC 3783, where ν_p is the Lorentzian peak frequency, Q is its quality factor, ν_B is the power law bend frequency and α_L and α_H are the power law slopes below and above the bend, respectively. The errors are calculated from the 68% confidence intervals, and an asterisk indicates that the limit is unconstrained.
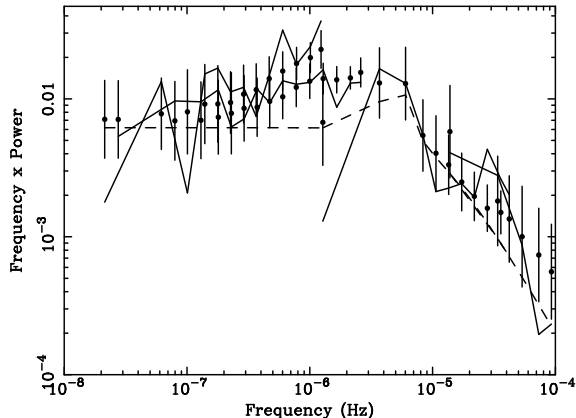

Figure 10. The best-fitting single-bend power law with a Lorentzian component. The fit was done using the entire data set but here we only show the Lorentzian region. As before, solid lines represent the real data PSD, dashed lines represent the best-fitting model and markers with error bars represent the model distorted by sampling effects. The Lorentzian feature in the model can reproduce qualitatively the spurious power at the high frequency end of the long-term monitoring data and the turn down effect observed in the intensive-sampling data.

significance of the double-bend model. We found that 222 of the 300 single-bend simulated PSDs have a higher fit probability than the data, when fitted with the single-bend power law plus Lorentzian model. This result indicates that the increase in fit probability could be due to the added complexity of the model, and that the improvement in the fit over a simple bending power law is not significant.

4 DISCUSSION AND CONCLUSIONS

We have combined our own new *RXTE* monitoring data with archival *RXTE* and *XMM-Newton* observations to construct a high-quality PSD of NGC 3783 spanning five decades in frequency.

We find that a 'soft' state model, with a single bend at 6.2×10^{-6} Hz, similar to that found earlier by Markowitz et al. (2003), a power law of slope approximately -0.8 extending over almost three decades in frequency below the bend, and slope above the bend of approximately -2.6 is a good fit to the data. We also find that a 'hard' state model, with a double bend, fits the data, as does a model with a single bend plus an additional Lorentzian component. However the improvement in fit is marginal and, given the additional free parameters, is not significant. Thus we conclude that a simple 'soft' state model provides the most likely explanation of the data.

Assuming a mass of $3 \times 10^7 M_\odot$ for NGC 3783 (Peterson et al. 2004), and an accretion rate of 7% of the Eddington limit (Uttley & McHardy 2005, based on Woo & Urry 2002), then NGC 3783 is still in good agreement with the scaling of PSD break timescale as $\sim M/\dot{m}_E$ between AGN and GBHs found by McHardy et al. (2006).

Our new fits, show that the PSD of NGC 3783 is perfectly consistent with a single-bend power law with low-frequency slope of -1, in contrast with the earlier result of Markowitz et al. (2003), who found that a similar model was rejected tentatively at $\sim 98\%$ confidence. The difference can be understood in terms of the improved long-term data. Our new *RXTE* monitoring observations occur every 2 days, compared to 4 days previously, thereby increasing the long term *RXTE* data set by a factor 2.6 and, in particular, providing overlap at high frequencies with the *RXTE* intensive monitoring data. The drop in long-timescale variability power, evident in the older long term monitoring data is not reproduced by the new long-term monitoring data, showing that this drop could be just a statistical fluctuation. In addition, the very high frequencies are better constrained by the 2 orbits of *XMM-Newton* data than by the earlier *Chandra* data used by Markowitz et al. (2003).

The classification of the PSD as being 'soft' state means that NGC 3783 is no longer considered unusual amongst AGN. The fact that this AGN is radio-quiet strongly supports the analogy with GBHs in the soft state. Also the accretion rate of NGC 3783 ($\dot{m}_E$ =0.07) (Uttley & McHardy 2005, based on Woo & Urry 2002) is similar to that of other AGN with soft-state PSDs (e.g. NGC 3227 Uttley & McHardy 2005, NGC 4051 McHardy et al. 2004, MCG-6-30-15 McHardy et al. 2005). This accretion rate is above the rate at which the persistent GBH Cyg X-1 transits between hard and soft states in either direction and at which other GBHs transit from the soft to hard state ($\dot{m}_E$ =0.02) (Maccarone et al. 2003; Maccarone 2003). We note that other transient GBHs in outburst, where the variable power law emission in the soft state PSD is weak, can remain in the hard state to much higher accretion rates ($\sim$ 2–50% Homan & Belloni 2005) but it is not clear whether we should expect similar PSD shapes to AGN for such outbursting sources. Thus NGC 3783 remains compatible with other moderately accreting AGN in being analogous to Cyg X-1 in the soft state. It is, of course, possible that the transition rate might not be independent of mass. Observations do not yet greatly constrain the transition rate as a function of mass but the abscence of large deviations from the so-called 'fundamental' plane of radio luminosity, X-ray luminosity and black hole mass (Merloni et al. 2003; Falcke et al. 2004) argues against a large spread in the transistion accretion-rates (e.g. see Körding et al. 2006). In the case of Seyfert galaxy

NGC 3227, the accretion rate is ~ 1–2% and a 'soft' state PSD is measured (Uttley & McHardy 2005), which suggests that the transition accretion-rate in AGN should be at or below that value.

Our observations, which show that NGC 3783 does not have a highly unusual PSD, therefore confirm the growing similarities between AGN and Galactic black hole systems and leave only Arakelian 564, which is probably a very high state object, as the only AGN showing clear double breaks (or multiple Lorentzians) in its PSD (e.g. Arévalo et al. 2006, McHardy et al. in prep.).

ACKNOWLEDGEMENTS

REFERENCES

Arévalo P., Papadakis I. E., Uttley P., McHardy I. M., Brinkmann W., 2006, MNRAS, 372, 401

Axelsson M., Borgonovo L., Larsson S., 2006, A&A, 452, 975

Belloni T., Homan J., Casella P., van der Klis M., Nespoli E., Lewin W. H. G., Miller J. M., Méndez M., 2005, A&A, 440, 207

Churazov E., Gilfanov M., Revnivtsev M., 2001, MNRAS, 321, 759

Corbel S., Fender R. P., Tzioumis A. K., Nowak M., McIntyre V., Durouchoux P., Sood R., 2000, A&A, 359, 251

Cui W., Heindl W. A., Rothschild R. E., Zhang S. N., Jahoda K., Focke W., 1997, ApJL, 474, L57+

Done C., Gierliński M., 2005, MNRAS, 364, 208

Edelson R., Nandra K., 1999, ApJ, 514, 682

Falcke H., Körding E., Markoff S., 2004, A&A, 414, 895

Fender R. P., 2001, MNRAS, 322, 31

Homan J., Belloni T., 2005, ApSS, 300, 107

Homan J., Wijnands R., van der Klis M., Belloni T., van Paradijs J., Klein-Wolt M., Fender R., Méndez M., 2001, ApJS, 132, 377

Körding E. G., Fender R. P., Migliari S., 2006, MNRAS, 369, 1451

Körding E. G., Jester S., Fender R., 2006, MNRAS, 372, 1366

Maccarone T. J., 2003, A&A, 409, 697

Maccarone T. J., Gallo E., Fender R., 2003, MNRAS, 345, L19

Markowitz A., 2005, ApJ, 635, 180

Markowitz A., Edelson R., Vaughan S., Uttley P., George I. M., Griffiths R. E., Kaspi S., Lawrence A., McHardy I., Nandra K., Pounds K., Reeves J., Schurch N., Warwick R., 2003, ApJ, 593, 96

McHardy I., 1988, Memorie della Societa Astronomica Italiana, 59, 239

McHardy I. M., Gunn K. F., Uttley P., Goad M. R., 2005, MNRAS, 359, 1469

McHardy I. M., Koerding E., Knigge C., Uttley P., Fender R. P., 2006, Nature, 444, 730

McHardy I. M., Papadakis I. E., Uttley P., Page M. J., Mason K. O., 2004, MNRAS, 348, 783

Merloni A., Heinz S., di Matteo T., 2003, MNRAS, 345, 1057

Nowak M. A., 2000, MNRAS, 318, 361

Nowak M. A., Vaughan B. A., Wilms J., Dove J. B., Begelman M. C., 1999, ApJ, 510, 874

Papadakis I. E., Brinkmann W., Negoro H., Gliozzi M., 2002, A&A, 382, L1

Papadakis I. E., Lawrence A., 1993, MNRAS, 261, 612

Peterson B. M., Ferrarese L., Gilbert K. M., Kaspi S., Malkan M. A., Maoz D., Merritt D., Netzer H., Onken C. A., Pogge R. W., Vestergaard M., Wandel A., 2004, ApJ, 613, 682

Pottschmidt K., Wilms J., Nowak M. A., Pooley G. G., Gleissner T., Heindl W. A., Smith D. M., Remillard R., Staubert R., 2003, A&A, 407, 1039

Pounds K., Edelson R., Markowitz A., Vaughan S., 2001, ApJL, 550, L15

Reig P., Papadakis I., Kylafis N. D., 2002, A&A, 383, 202

Revnivtsev M., Gilfanov M., Churazov E., 2000, A&A, 363, 1013

Reynolds C. S., 1997, MNRAS, 286, 513

Timmer J., Koenig M., 1995, A&A, 300, 707

Uttley P., McHardy I. M., 2005, MNRAS, 363, 586

Uttley P., McHardy I. M., Papadakis I. E., 2002, MNRAS, 332, 231

Uttley P., McHardy I. M., Vaughan S., 2005, MNRAS, 359, 345

Wilms J., Nowak M. A., Pottschmidt K., Pooley G. G., Fritz S., 2006, A&A, 447, 245

Woo J.-H., Urry C. M., 2002, ApJ, 579, 530

Zhang W., Giles A. B., Jahoda K., Soong Y., Swank J. H., Morgan E. H., 1993, in Siegmund O. H., ed., Proc. SPIE Vol. 2006, p. 324-333, EUV, X-Ray, and Gamma-Ray Instrumentation for Astronomy IV, Oswald H. Siegmund; Ed. Laboratory performance of the proportional counter array experiment for the X-ray Timing Explorer. pp 324–333